ISSN 1063-7761, Journal of Experimental and Theoretical Physics, 2019, Vol. 129, No. 6, pp. 1062–1069. © Pleiades Publishing, Inc., 2019.
Russian Text © The Author(s), 2019, published in Zhurnal Eksperimental'noi i Teoreticheskoi Fiziki, 2019, Vol. 156, No. 6, pp. 1165–1174.

ORDER, DISORDER, AND PHASE TRANSITION IN CONDENSED SYSTEM

Magnetic Properties and Spin Crossover in Transition Metal Oxides with d^5 Ions at High Pressures

Yu. S. Orlov[a],*, S. V. Nikolaev[a], and S. G. Ovchinnikov[b]

[a] *Kirensky Institute of Physics, Federal Research Center "Krasnoyarsk Science Center," Russian Academy of Sciences, Krasnoyarsk, 660036 Russia*

[b] *Siberian Federal University, Krasnoyarsk, 660041 Russia*

**e-mail: jso.krasn@mail.ru*

Received June 26, 2019; revised August 22, 2019; accepted August 27, 2019

Abstract—We analyze the influence of cooperative effects on the magnetic properties and spin crossover between the high-spin (HS) term $S = 5/2$ and low-spin (LS) term $S = 1/2$ in Mott–Hubbard dielectrics with $3d^5$ ions under high pressures. Two cooperation mechanisms (superexchange interaction and effective interaction via the elastic system) are considered. The sign of the exchange interaction changes because of the crossover from the antiferromagnetic in the HS state to the ferromagnetic in the LS state. In view of the large difference between the ionic radii of the HS and LS states, the systems with spin crossover acquire an additional strong coupling via the elastic system. Using the Hubbard operator representation and considering the electronic states of the two terms simultaneously, we obtain the effective Hamiltonian with allowance for the cooperative effects. The magnetic phase diagram and the spin crossover are investigated in the mean field approximation. It is shown that the inclusion of cooperative effects at low temperatures leads to a first-order phase transition between the antiferromagnetic HS state and the ferromagnetic LS state. At higher temperatures, more complicated sequences of phase transitions are possible upon an increase in pressure, including the HS paramagnet–HS antiferromagnet–LS paramagnet and HS antiferromagnet–LS paramagnet–LS ferromagnet transitions.

DOI: 10.1134/S1063776119120185

1. INTRODUCTION

In the magnetism of dielectrics, only the ground energy levels of magnetic ions with certain values of the spin, orbital, and total magnetic moments are traditionally considered, and the adequate low-energy model for their description is the Heisenberg model. At the same time, in a large number of recent publications, there appear spin crossover (SC) effects associated with crossing of two terms of a cation with different spin states [1]. Spin crossover can be observed in oxides of $3d$ metals with configurations d^4–d^7 [2–4] and in organometallic complexes [5]. These materials can form the basis in constructing inertia-free molecular switches for data storage and quick processing. In nanotechnology, materials with SC are used for quantum transport in new-generation sensors [6]. Processes with SC in Fe-containing oxides are also important for understanding physical properties in the depth of the Earth mantle [7–10].

Spin crossover appears due to the competition between the intraatomic Hund exchange interaction, which stabilizes the HS state, and the crystal field energy, which is minimal for the LS state. This is a one-ion process described by the Tanabe–Sugano diagrams. At the same time, crystals also exhibit cooperative effects associated with interactions between ions (e.g., the exchange interaction). The effect of the interatomic exchange between d^6 ions in the HS state has been considered recently in [11], where the LS state is characterized by $S = 0$ and is nonmagnetic. In this study, we analyze the effect of cooperation in oxides with d^5 ions, which corresponds to the Fe^{3+} ion in oxides that are magnetic at room temperature, such as Fe_2O_3, $FeBO_3$, $RFeO_3$ (R is a rare-earth element), $BiFeO_3$, $Y_3Fe_5O_{12}$, as well as $GdFe_3(BO_3)_4$, for which the Néel temperature is lower than 77 K [1]. Oxides with d^5 ions also include MnO. We intentionally single out oxides that are magnetic and nonmagnetic at room temperature, because it is more convenient to perform experiments on the Mössbauer effect and X-ray emission spectra (XES) under megabar pressures on diamond anvils at room temperature. Experiments at low temperatures are also possible, but are much more complicated [12]. To describe the magnetism in SC systems theoretically, it is necessary to exceed the limits of the low-energy Heisenberg model and to consider the contributions of both HS and LS terms to the effective low-energy Hamiltonian. In addition, the large difference in the ionic radii (by approximately 10%) of HS and LS ions necessitates the inclusion of

the additional specific cooperation mechanism associated with the indirect interaction of cations via the elastic system.

This article has the following structure. In Section 2, we consider the effective low-energy Hamiltonian with allowance for two magnetic terms at each ions and with the interaction with vibronic oscillations, as well as equations in the mean field theory. In this problem, the most adequate mathematical language is that with the Hubbard operators; in the representation of these operators, the initial multiband p–d model with allowance for electronic d states of cations and p states of anions, as well as all strong Coulomb interactions in the LDA + GTB approach [13], is projected onto the effective low-energy model with selected multielectron terms. This procedure was describe in detail in [11] and is generalized here to the case of two magnetic terms of the cation. In Section 3, the results of calculation of the phase diagram on the (pressure, temperature) plane are considered.

2. EFFECTIVE HAMILTONIAN OF MAGNETICALLY ORDERED DIELECTRICS WITH SPIN CROSSOVER

The effective Hamiltonian describing the effect of the exchange interaction on spin crossover in magnetically ordered dielectrics under pressure with allowance for the vibronic interaction in the representation of the Hubbard X operators constructed on states with different spin projections $|s_\alpha^z\rangle$, $s_\alpha^z = -S_\alpha, -S_\alpha + 1, \ldots, +S_\alpha$, where $\alpha = 1, 2$ for HS and LS, respectively, can be written as

$$\hat{H}_{\text{eff}} = \hat{H}^{(S)} + \hat{H}^{(e,q)}. \quad (1)$$

Here, the first term

$$\hat{H}^{(S)} = \sum_{\langle i,j\rangle}\sum_{\alpha,\beta}\left(J_{\alpha\beta}\hat{\mathbf{S}}_i^\alpha\hat{\mathbf{S}}_j^\beta - \frac{1}{4}\hat{n}_i^\alpha\hat{n}_j^\beta\right) + \Delta_S\sum_{i,s_2^z}X_i^{s_2^z,s_2^z} \quad (2)$$

contains exchange interaction $J_{\alpha\beta}$ (α, β = 1, 2) with account for the change in the relative energy of the electron configurations of LS and HS states under the effect of applied pressure P; $\hat{\mathbf{S}}_i^\alpha$ are the spin operators for $S_1 = 5/2$ ($\alpha = 1$) and $S_2 = 1/2$ ($\alpha = 2$):

$$\hat{S}_{1i}^+ = \sqrt{5}X_i^{-3/2,-5/2} + 2\sqrt{2}X_i^{-1/2,-3/2} + 3X_i^{+1/2,-1/2} + 2\sqrt{2}X_i^{+3/2,+1/2} + \sqrt{5}X_i^{+5/2,+3/2},$$

$$\hat{S}_{1i}^- = \sqrt{5}X_i^{-5/2,-3/2} + 2\sqrt{2}X_i^{-3/2,-1/2} + 3X_i^{-1/2,+1/2} + 2\sqrt{2}X_i^{+1/2,+3/2} + \sqrt{5}X_i^{+3/2,+5/2},$$

$$\hat{S}_{1i}^z = -\frac{5}{2}X_i^{-5/2,-5/2} - \frac{3}{2}X_i^{-3/2,-3/2} - \frac{1}{2}X_i^{-1/2,-1/2} + \frac{1}{2}X_i^{+1/2,+1/2} + \frac{3}{2}X_i^{+3/2,+3/2} + \sqrt{5}X_i^{+5/2,+5/2},$$

[14], and analogously, for S_2,

$$\hat{n}_i = 5\sum_{s_1^z=-S_1}^{+S_1}X_i^{s_1^z,s_1^z} + 5\sum_{s_2^z=-S_2}^{+S_2}X_i^{s_2^z,s_2^z}$$

is the operator of the number of particles at the ith site. In view of the condition of completeness for the Hubbard X operators, we have

$$\sum_{s_1^z=-S_1}^{+S_1}X^{s_1^z,s_1^z} + \sum_{s_2^z=-S_2}^{+S_2}X^{s_2^z,s_2^z} = 1, \quad \langle\hat{n}_i\rangle = 5.$$

In expression (2), $\Delta_S = E_{LS} - E_{HS}$ is the spin gap width (energy interval between the LS and HS states). Henceforth, we will assume the linear dependence of the crystal field and Δ_S on pressure, $\Delta_S = a(P_{C0} - P)$, where P_{C0} is the critical pressure for which $\Delta_S = 0$, and crossover could occur in the absence of cooperative effects, as well as the linear dependence of exchange integral $J_{\alpha\beta}$ on pressure [1]:

$$J_{\alpha\beta}(P) = \begin{pmatrix} J_{HS}^0 + b_{HS}P & -J_{12} \\ -J_{12} & -(J_{LS}^0 + b_{LS}P) \end{pmatrix}.$$

The sign reversal of the exchange interaction from the antiferromagnetic at low pressures to the ferromagnetic above the crossover point for crystals with d^5 terms was predicted in [15]. The second term contains the energy of fully symmetric molecular vibrations, the electron-vibrational (vibronic) interaction, and the elastic interaction of cations of the 3d metal at neighboring crystal lattice sites and describes the variation of the system volume upon a change in temperature and external pressure [16, 17]:

$$\hat{H}^{(e,q)} = \sum_i\left(\frac{1}{2}k\hat{q}_i^2 + \frac{\hat{p}_i^2}{2M}\right) - \sum_i(g_1\hat{q}_i + g_2\hat{q}_i^2) \times\left(-\sum_{s_1^z=-S_1}^{+S_1}X_i^{s_1^z,s_1^z} + \sum_{s_2^z=-S_2}^{+S_2}X_i^{s_2^z,s_2^z}\right) - \frac{1}{2}V_g\sum_{\langle i,j\rangle}\hat{q}_i\hat{q}_j, \quad (3)$$

where g_1 and g_2 are the intramolecular electron-vibrational interaction constants; k is the elastic coupling constant; $\hat{q}_i$ is the operator of the normal coordinate, which corresponds to the breathing mode of ligand vibrations and momentum operator $\hat{p}_i$ conjugate to it; V_q is the elastic intermolecular interaction constant, and M is the effective mass of the oscillator. Since the natural frequencies of ligand vibrations in the LS and HS states are different,

$$\omega_{LS(HS)} = \sqrt{\frac{k_{LS(HS)}}{M}},$$

it is necessary to consider not only linear but also quadratic in $\hat{q}$ terms in the electron-vibrational interaction. The elastic coupling constants in the LS and HS states are $k_{LS} = k + 2g_2$ and $k_{HS} = k - 2g_2$, respectively.

In the mean field approximation, Hamiltonian (1) has form

$$\hat{H}_{MF} = H_0 - \sum_{i,\alpha} \mathbf{B}_\alpha \hat{\mathbf{S}}_i^\alpha + \Delta_S \sum_{i,s_2^z} X_i^{s_2^z,s_2^z} + \sum_i \left(\frac{1}{2} k \hat{q}_i^2 + \frac{\hat{p}_i^2}{2M} \right) - \sum_i (g_1 \hat{q}_i + g_2 \hat{q}_i^2) \times \left(- \sum_{s_1^z=-S_1}^{+S_1} X_i^{s_1^z,s_1^z} + \sum_{s_2^z=-S_2}^{+S_2} X_i^{s_2^z,s_2^z} \right) - V_q \langle \hat{q} \rangle \sum_i \hat{q}_i. \quad (4)$$

Here,

$$\mathbf{B}_\alpha = z \sum_\beta J_{\alpha\beta} \langle \hat{\mathbf{S}}^\beta \rangle$$

is the Weiss field, where $z = 6$ is the number of the nearest neighbors, and $m = \langle \hat{S}_1^z \rangle + \langle \hat{S}_2^z \rangle$ is the mean projection of the sublattice spin.

Let us consider the representation of Hamiltonian operator (4) in matrix form using the orthonormal basis of functions in the form of the direct product of eigenstates of spin projection operators $|s_\alpha^z\rangle$ and of harmonic oscillator $|n_{ph}\rangle$:

$$|s_\alpha^z, n_{ph}\rangle = |s_\alpha^z\rangle |n_{ph}\rangle, \quad n_{ph} = 0,1,2,\ldots.$$

To do this, it is convenient to use the expressions for the operators of displacement,

$$\hat{q}_i = \sqrt{\frac{\hbar}{2M\omega}} (a_i + a_i^\dagger)$$

and momentum,

$$\hat{p}_i = \frac{1}{i} \sqrt{\frac{\hbar M \omega}{2}} (a_i - a_i^\dagger)$$

in the secondary quantization representation, which gives

$$|n_{ph}\rangle = \frac{1}{\sqrt{n_{ph}!}} (a^\dagger)^{n_{ph}} |0,0,\ldots,0\rangle$$

and

$$H_{\alpha,s_\alpha^z,n_{ph}}^{\alpha',s_\alpha'^z,n_{ph}'} = \left\{ \left[-\frac{\Delta_S}{2} - \frac{g_2 \hbar\omega}{2k} (2n_{ph}+1) \right] \lambda_\alpha + \hbar\omega \left(n_{ph} + \frac{1}{2} \right) - s_\alpha^z z \sum_\beta J_{\alpha\beta} \langle \hat{S}_\beta^z \rangle + \frac{H_0}{N} \right\} \times \delta_{\lambda_\alpha,\lambda_{\alpha'}} \delta_{s_\alpha^z s_\alpha'^z} \delta_{n_{ph} n_{ph}'} - \lambda_\alpha g_1 \sqrt{\frac{\hbar\omega}{2k}} \times (\sqrt{n_{ph}} \delta_{n_{ph}-1,n_{ph}'} + \sqrt{n_{ph}+1} \delta_{n_{ph}+1,n_{ph}'}) \times \delta_{\lambda_\alpha\lambda_{\alpha'}} \delta_{s_\alpha^z s_\alpha'^z} - \lambda_\alpha g_2 \frac{\hbar\omega}{2k} \left(\sqrt{n_{ph}(n_{ph}-1)} \delta_{n_{ph}-2,n_{ph}'} + \sqrt{(n_{ph}+2)(n_{ph}+1)} \delta_{n_{ph}+2,n_{ph}'} \right) \delta_{\lambda_\alpha\lambda_{\alpha'}} \delta_{s_\alpha^z s_\alpha'^z} - V_q \langle \hat{q} \rangle \sqrt{\frac{\hbar\omega}{2k}} \times (\sqrt{n_{ph}} \delta_{n_{ph}-1,n_{ph}'} + \sqrt{n_{ph}+1} \delta_{n_{ph}+1,n_{ph}'}) \quad (5)$$

where N is the number of lattice sites and $\lambda_\alpha = 1$ if $\alpha = 1$ and $\lambda_\alpha = -1$ if $\alpha = 2$.

The set of eigen wavefunctions can be written as

$$|\varphi_k\rangle = \sum_{n_{ph}=0}^{N_{ph}} \left[\sum_{s_2^z=-S_2}^{+S_2} a_{n_{ph},s_2^z,k} |s_2^z, n_{ph}\rangle + \sum_{s_1^z=-S_1}^{+S_1} b_{n_{ph},s_1^z,k} |s_1^z, n_{ph}\rangle \right], \quad (6)$$

where N_{ph} is the number of phonons beginning from which (for $n_{\text{ph}} > N_{\text{ph}}$ and a preset intensity of the electron-vibrational interaction) the energy

$$E_0(N_{ph}+1) \approx E_0(N_{ph})$$

of the ground state $|\varphi_0\rangle$ stops changing, and weight coefficients are given by

$$a_{n_{ph},0}(N_{ph}+1) \approx a_{n_{ph},0}(N_{ph}),$$

$$b_{n_{ph},s_z,0}(N_{ph}+1) \approx a_{n_{ph},s_2,z}(N_{ph}).$$

In analysis of various temperature effects, it is necessary to trace the constancy of energy E_k of excited states $|\varphi_k\rangle$ that are closest to the ground state and of weight coefficients

$$a_{n_{ph},k}(N_{ph}+1) \approx a_{n_{ph},k}(N_{ph}),$$

$$b_{n_{ph},s_z,k}(N_{ph}+1) \approx b_{n_{ph},s_z,k}(N_{ph}).$$

In other words, N_{ph} defines the number of phonons that must be taken into account for a given intensity of the electron-vibrational interaction for the "phonon coat" to be formed. In our calculations, $N_{\text{ph}} = 300$–500, depending on the values of parameters, as well as on pressure and temperature used. Then the quantum-mechanical mean values of spin projection operator $\hat{S}^z$, displacement operator $\hat{q}$, and occupancy $\hat{n}$ of the HS state are given by

$$\langle \hat{n} \rangle_k = \left\langle \varphi_k \left| \sum_{s_1^z=-S_1}^{+S_1} X^{s_1^z,s_1^z} \right| \varphi_k \right\rangle = \sum_{n_{ph}=0}^{N_{ph}} \sum_{s_1^z=-S_1}^{+S_1} |b_{n_{ph},s_1^z,k}|^2, \quad (7)$$

$$\langle\hat{q}\rangle_k = \langle\varphi_k|\hat{q}|\varphi_k\rangle = \sqrt{\frac{\hbar}{2M\omega}} \times\sum_{n_{ph}=0}^{N_{ph}}\left\{\sqrt{n_{ph}}\left(\sum_{s_2^z=-S_2}^{+S_2} a_{n_{ph},s_2^z,k}a_{n_{ph}-1,s_2^z,k} + \sum_{s_1^z=-S_1}^{+S_1} b_{n_{ph},s_1^z,k}b_{n_{ph}-1,s_1^k,k}\right)\right. \left.+\sqrt{n_{ph}+1}\left(\sum_{s_1^z=-S_1}^{+S_2} a_{n_{ph},s_2^z,k}a_{n_{ph}+1,s_2^k,k} + \sum_{s_1^z=-S_1}^{+S_1} b_{n_{ph},s_1^z,k}b_{n_{ph}+1,s_1^k,k}\right)\right\}, \quad (8)$$

$$\langle\hat{S}_1^z\rangle_k = \langle\varphi_k|\hat{S}_1^z|\varphi_k\rangle = \sum_{n_{ph}=0}^{N_{ph}}\sum_{s_1^z=-S_1}^{+S_1} s_1^z|b_{n_{ph},s_1^z,k}|^2,$$
$$\langle\hat{S}_2^z\rangle_k = \langle\varphi_k|\hat{S}_2^z|\varphi_k\rangle = \sum_{n_{ph}=0}^{N_{ph}}\sum_{s_2^z=-S_2}^{+S_2} s_2^z|a_{n_{ph},s_2^z,k}|^2. \quad (9)$$

Accordingly, their quantum-statistical mean values are given by

$$n = \langle\hat{n}\rangle = \sum_k \frac{\langle\hat{n}\rangle_k e^{-E_k/k_BT}}{Z}, \quad (10)$$

$$q = \langle\hat{q}\rangle = \sum_k \frac{\langle\hat{q}\rangle_k e^{-E_k/k_BT}}{Z}, \quad (11)$$

$$\langle\hat{S}_\alpha^z\rangle = \sum_k \frac{\langle\hat{S}_\alpha^z\rangle_k e^{-E_k/k_BT}}{Z}, \quad (12)$$

where $Z = \sum_k e^{-E_k/k_BT}$ is the partition function.

The equilibrium positions of ligands corresponding to the minima of the potential energy of vibrations of the SC complex in the LS and HS states are defined by expressions

$$q_{LS}^0 = -\frac{g_1}{k_{LS}} \quad \text{and} \quad q_{HS}^0 = \frac{g_1}{k_{HS}},$$

respectively. For the chosen values of parameters that will be given below, $q_{LS}^0 = -0.09$ Å, $q_{HS}^0 = 0.13$ Å, and $\Delta q^0 = q_{HS}^0 - q_{LS}^0 = 0.22$ Å. Considering that the length of the bond at $T = 0$ is approximately 2 Å, we find that Δq^0 amounts to 10% of this value. This value is in conformity with the known difference in the ionic radii in the LS and HS states. It can be seen that $q_{LS(HS)}^0 = 0$ in the absence of the electron-vibrational interaction, and the volume of the system can change upon an increase in temperature only because of anharmonism.

3. P–T PHASE DIAGRAM

We can write the unit cell volume as a function of pressure and temperature in form

$$V(P,T) = V_r(P,T) + \Delta V(P,T),$$

where $V_r(P, T)$ is the regular component associated with anharmonism of lattice vibrations and $\Delta V(P, T) \sim q^3$ is the anomalous contribution appearing because of the vibronic interaction. In addition, for materials with spin crossover, a large contribution to the thermal expansion anomaly comes from the distribution of statistical weights HS/LS due to the large difference in their ionic radii [18]. Let us first consider the solutions to system of equations (5) and (10)–(12) in the absence of the exchange interaction, $J_{\alpha\beta} = 0$. In this case, we have $m = 0$ for magnetization and a sharp jump in population n of the HS state and in displacement q (unit cell volume) at the crossover point at $T = 0$, which corresponds to a quantum phase transition at point P_{C0} [19]. For $J_{\alpha\beta} = 0$, the quantum phase transition is blurred upon an increase in temperature into a smooth crossover between the HS and LS states (Fig. 1). For convenience of comparison of the cases with $J_{\alpha\beta} = 0$ and $J_{\alpha\beta} \neq 0$, we express here and below the pressure and temperature in the units of P_{C0} and exchange interaction J_{HS}^0, respectively.

Figures 2a, 2b, and 2c show the diagrams of population n of the HS state, magnetization m. and displacement q, respectively, which are the self-consistent solution to systems of equations (5) and (10)–(12) for $J_{\alpha\beta} \neq 0$. For preset values of temperature and pressure, there can appear several solutions for parameters n, m, and q, from which we choose the solutions corresponding to the minimum of Helmholtz free energy $F = -k_BT\ln Z$. Calculations were performed for the following values of parameters typical of $FeBO_3$ [20]: $z = 6$, $a = 80$ K GPa^{-1}, $P_{C0} = 55$ GPa, $k = 7.5$ eV/Å^2, $\omega = 0.05$ eV, $g_1 = 0.8$ eV/A, $g_2 = 0.75$ eV/Å^2, $J_{HS}^0 = 20.3$ K ($S_1 = 5/2$), $b_{HS} = 0.3$ K GPa^{-1}, $J_{LS}^0 = 13$ K ($S_2 = 1/2$), $b_{LS} = 0.4$ K GPa^{-1}, $J_{12} = 0$, and $V_q = 0.2$ eV/A. It can be seen that because of the cooperative exchange interaction $J_{\alpha\beta}$, the ground magnetically ordered antiferromagnetic HS state, AFM (HS), is preserved in the system up to $P = P_C > P_{C0}$ (see Fig. 2b) in spite of the fact that the LS state is the ground state in the one-ions situation at $P > P_{C0}$. The shift of critical pressure due to cooperative effects is not surprising, because the exchange interaction stabilizes the HS state more strongly. At $P > P_C$, the ground antiferromagnetic HS state changes to the ferromagnetic LS state, FM (LS) (see Fig. 2b), and the volume experiences a jump at transition point $P = P_C$ (see Fig. 2c).

In pressure range $P < P_C$ (see Fig. 2b), with increasing temperature, the system experiences a second-order phase transition from the AFM (HS) state to the

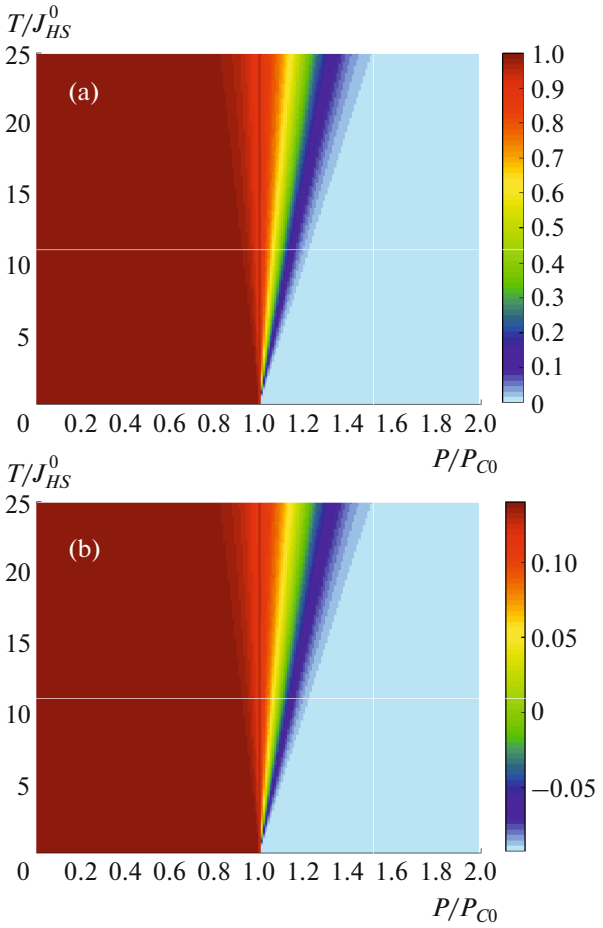

Fig. 1. (Color online) Diagram of (a) population n of the HS state and (b) displacement q in the absence of exchange interaction $J_{\alpha\beta} = 0$.

paramagnetic state if $P < P^*$ and a first-order transition if $P^* < P < P_C$. In the former case, a smooth variation of the volume is observed, while, in the latter case, conversely, the volume changes abruptly (see Fig. 2c). The P–T diagrams clearly show a singular point, a so-called tricritical point (T^* and P^* in Fig. 2b), at which the second-order phase transition curve is continuously transformed into the first-order transition curve.

In pressure range $P > P_C$, the system experiences a second-order phase transition from the ferromagnetic (LS) to the paramagnetic state upon an increase in temperature; with increasing pressure, an increase in the Curie temperature is observed.

Because of an increase in the exchange integral with increasing pressure, recurrent magnetization in pressure can appear at $T_0 < T \le T'$, where T_0 is the Néel temperature at $P = 0$ and T' is the maximal possible value of the Néel temperature upon an increase in pressure. For example, at $T_0 < T \le T'$ (see Fig. 2b), the system passes upon an increase of pressure first to

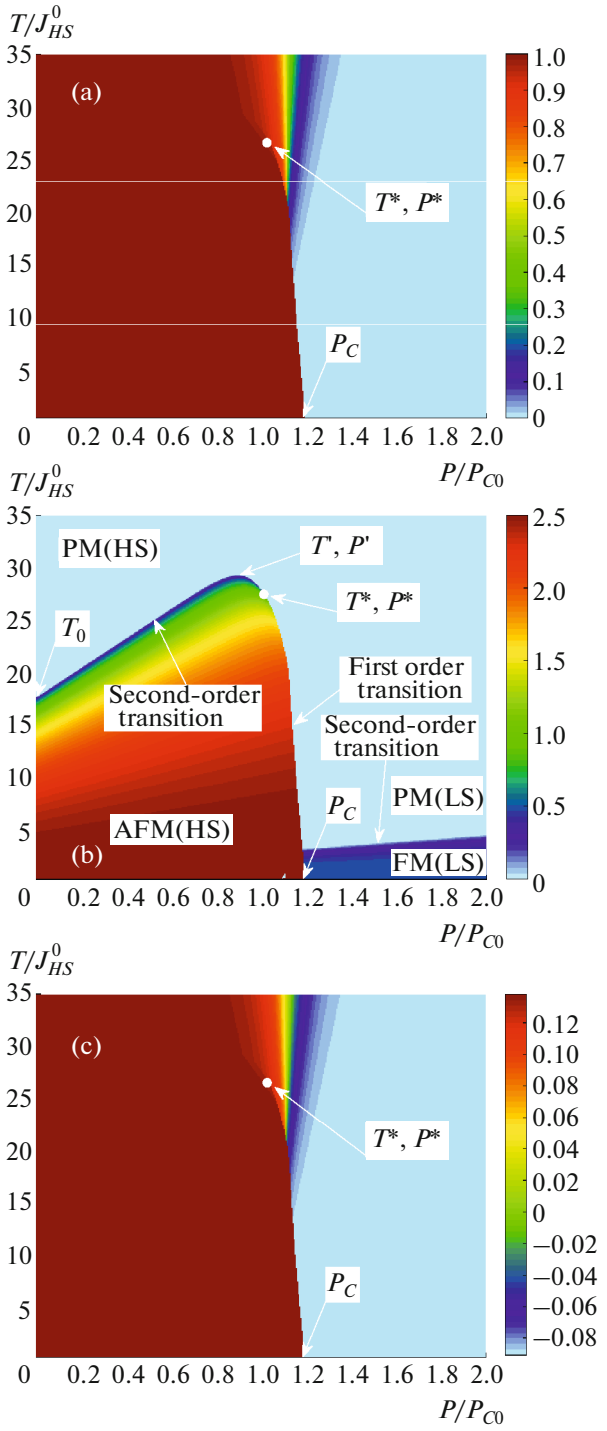

Fig. 2. (Color online) Diagram of (a) population n of the HS state, (b) magnetization m, and (c) displacement q corresponding to the minimum of free energy F.

the magnetically disordered antiferromagnetic state via a second-order transition and then to the paramagnetic state via a second-order transition if $T^* < T_0$ or a first-order transition if $T^* > T_0$, but $T^* < T < T'$. In our case, $T^* > T_0$ for the set of parameters being used. For

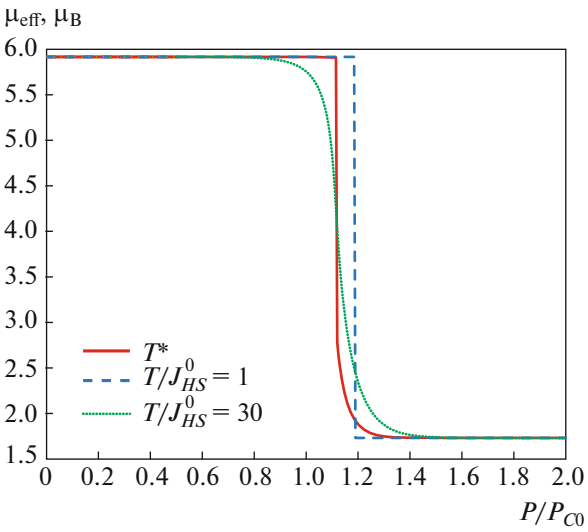

Fig. 3. (Color online) Dependence of effective magnetic moment $\mu_{eff}(P, T)$ on pressure P at different fixed values of T.

$0 \le T \le T^*$, the volume of the system changes jumpwise with increasing pressure, while at $T > T^*$, it changes continuously (see Fig. 2c).

Figures 3 and 4 show the dependence of effective magnetic moment

$$\mu_{eff}(P,T) = \mu_B g\sqrt{nS_1(S_1+1) + (1-n)S_2(S_2+1)}$$

on pressure P and temperature T in the units of Bohr magneton μ_B ($g = 2$ is the Lande factor) at different fixed values of T and P, respectively. In pressure range $0 \le P \le P'$, the effective magnetic moment decreases gradually with increasing pressure from the maximum possible value

$$\mu_{eff}^{HS} = \mu_B g\sqrt{S_1(S_1+1)} = 5.92\mu_B$$

(Fig. 4a). At $P' \le P \le P^*$, a kink is observed on temperature dependence $\mu_{eff}(P, T)$ (Fig. 4b), while at $P^* < P < P_C$, a sharp jump is observed (Fig. 4c); the temperatures corresponding to the kink and the jump are displaced with increasing pressure towards lower temperatures. Finally, in the LS phase above critical pressure P_C, a smooth increase in the effective magnetic moment with increasing temperature from the minimal possible value

$$\mu_{eff}^{HS} = \mu_B g\sqrt{S_2(S_2+1)} = 1.73\mu_B$$

is observed again without singularities.

4. CONCLUSIONS

In spite of the fact that the exchange Hamiltonian is of the Heisenberg form, the thermodynamics in the given problem is not standard, in which the magnetization is written in the form of the Brillouin function of the effective magnetic field. This difference, first, is due to the existence of two magnetic terms, each of which can be partly filled, and second, because the wavefunction is not the product of functions of each term. The condition of completeness of the multielectron Hilbert space requires that the sum of all diagonal Hubbard operators equal unity for both values of spin. This relation is preserved in our version of the mean field theory. The magnetic phase diagram and spin crossover have been analyzed in the mean field approximation. It is shown that at low temperatures, the account for cooperation leads to a first-order phase transition between the antiferromagnetic HS state and the ferromagnetic LS state. At higher temperatures, more complicated sequences of phase transitions are possible upon an increase in pressure, including the HS paramagnet–HS antiferromagnet–LS paramagnet and HS antiferromagnet–LS paramagnet–LS ferromagnet transition.

As noted in Introduction, there exist about ten different oxides with d^5 ions (mainly, compounds with the Fe^{3+} ion), which exhibit spin crossover [1]. The properties of $FeBO_3$ under pressure have been investigated most thoroughly. For instance, an increase in Néel temperature $T_N(P)$ was detected from the measurements of magnetization [21] and the two-magnon excitation frequency shift in the Raman spectra [22]. A sharp jump in the Néel temperature and suppression of the hyperfine field were observed in Mössbauer experiments [23], which was called by magnetic collapse by the authors of [23]. This collapse is accompanied with a jumpwise change in the volume [24] and a jump of the optical absorption edge with a dielectric (gap $E_g = 3$ eV)–semiconductor ($E_g = 0.7$ eV) transition [25]. A relationship between the magnetic collapse and the spin crossover of localized multielectron terms of the Fe^{3+} ion was proposed in [26, 27]. The experimental phase diagram of $FeBO_3$ was obtained and discussed in [20]. In this study, we combined analysis of magnetic and elastic properties in the vicinity of spin crossover associated with cooperative effects that were disregarded earlier. As can be seen from Fig. 2, the spin crossover and the volume jump occur simultaneously in conformity with experiment. Let us consider possible experiments that can shed light on the spin crossover physics. Analysis of elastic properties in a wide range of temperatures and pressures also ensures such opportunities, since the change in the ionic radius by approximately 10% due to the HS–LS crossover is manifested in macroscopic properties as a change in volume; for this reason, the charts of population and ion displacements in Figs. 2a and 2c are so similar. At the same time, X-ray diffraction experiments performed at various temperature and pressure are simpler than magnetic measurements using Mössbauer spectroscopy or X-ray magnetic circular dichroism. Therefore, it would be interesting to analyze the pressure dependences of crystal volume at different temperatures (above and below the tricritical point in

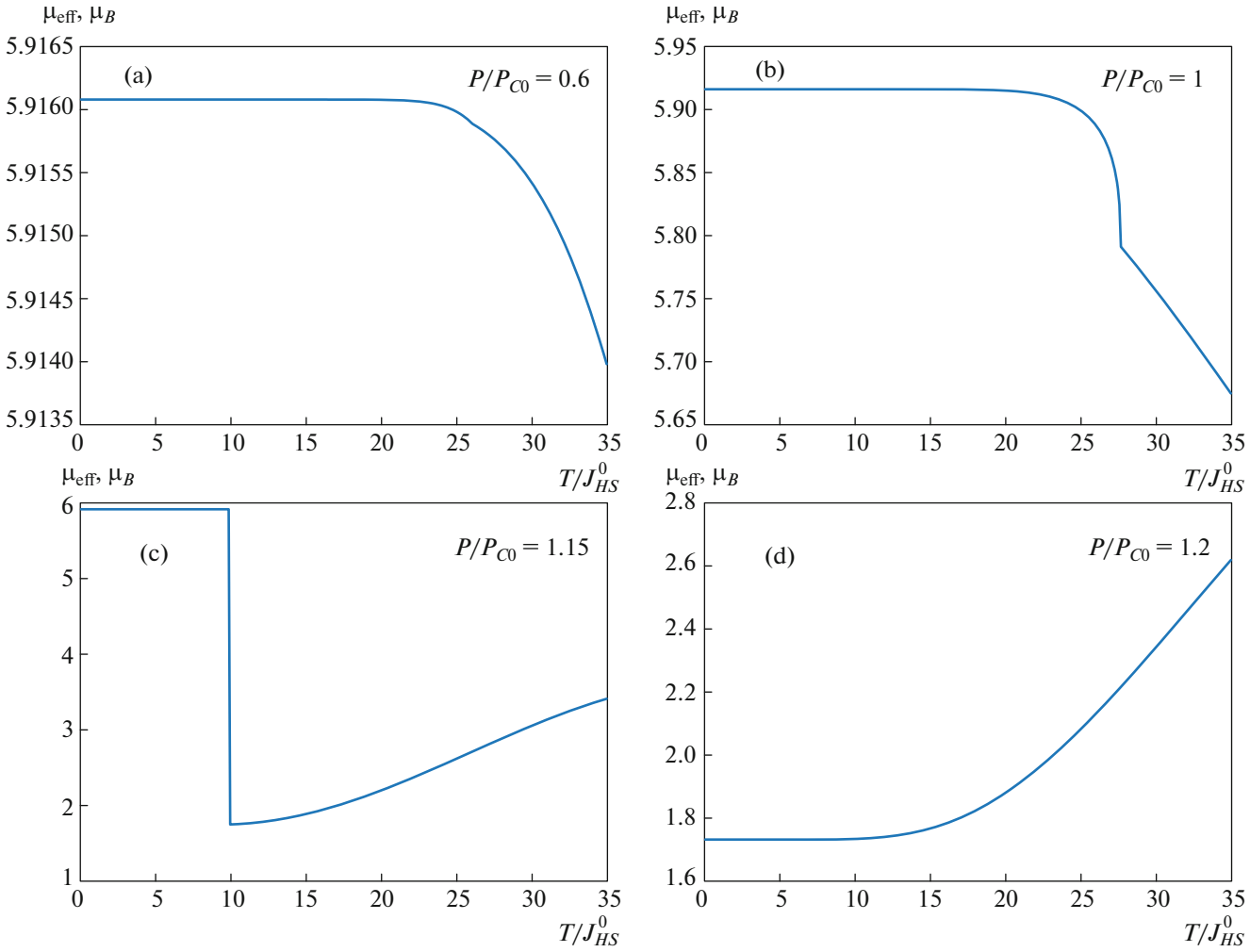

Fig. 4. (Color online) (a–d) Dependence of effective magnetic moment $\mu_{eff}(P, T)$ on temperature T at different fixed values of P.

Fig. 2). In particular, the tricritical point for $FeBO_3$ in Fig. 2 is close to room temperature. One can expect that the volume as a function of pressure at temperatures 77–100 K will change jumpwise at the spin crossover point as a result of the first-order phase transition, while at 350–400 K, the volume will vary smoothly in the pressure interval of width 10 GPa. One can also expect a difference in the behavior of heat capacity. During the first-order phase transition, an entropy jump occurs; for this reason, heat capacity measurements near the transition may give a significant increase at the crossover point (which is infinitely large in theory, but finite in experiment). The change in volume will obviously be manifested in the phonon frequency shift, which can be detected from the measurements of Raman spectra.

We can now assume that the properties of the HS state at pressures lower than P_C are quite clear. The increase in $T_N(P)$ observed from the Mössbauer spectral data coincides quantitatively with earlier data [21, 22]. The properties of the LS state at pressures exceeding P_C are not completely clear. Theoretical calculations of the electronic structure and magnetic properties above the critical pressure, which were based on the band theory, predicted the homogeneous antiferromagnetic phase with a magnetic moment of approximately one-fourth of that at zero pressure [28]. In analysis of the phase diagram [20], it was also assumed that the LS state at pressures above P_C is antiferromagnetic, and its Néel temperature is close to 50 K, which is much lower than in the high-spin state. In fact, the measurement of hyperfine fields does not allow one to distinguish between the antiferromagnetic and ferromagnetic phases. Therefore, the subsequent multielectron calculations of the exchange interaction [15], that have demonstrated the sign reversal of the exchange interaction during crossover, do not contradict the available Mössbauer data. The magnetic order type has not yet been determined experimentally. It is interesting to note that the magnetic moment ratio in the HS/LS states, which was represented in Fig. 3 for

the ferromagnetic phase, is close to a ratio of 1/4 predicted in [28] for the antiferromagnetic phase.

Another interesting feature in the behavior of Mott–Hubbard dielectrics upon a further increase in pressure is associated with the dielectric–metal transition and the role of spin crossover in this transition. It was shown in the multielectron model [29] that spin crossover in $FeBO_3$ suppresses Hubbard parameter U to almost one-third, which is reflected in the observed jump of the absorption edge [25]. Extrapolation of the pressure dependence of the gap above P_C has made it possible to estimate the probable metallization at pressures of about 210 GPa. It should be noted that the model of crossover in $FeBO_3$ considered here stops operating at pressure $P \approx 200$ GPa, for which the change in regimes from the Mott–Hubbard dielectric to the Kondo lattice and metallization are predicted [20]. Measurements of electric properties at such pressures [30] confirmed the metallic properties and manifestation of the Kondo lattice properties. Since electric properties can now be measured up to 300 GPa and higher on diamond anvils, which has made it possible to observe high-temperature superconductivity in hydrogen sulfide and metal hydrides [31–33], possible superconductivity of former Mott dielectrics at pressures exceeding 200 GPa is of certain interest.

FUNDING

This study was supported by the Russian Science Foundation (project no. 18-12-00022).

REFERENCES

1. I. S. Lyubutin and A. G. Gavriliuk, Phys. Usp. **52**, 989 (2009).
2. Y. Tanabe and S. Sugano, J. Phys. Soc. Jpn. **9**, 753 (1954).
3. I. Ohkoshi, K. Imoto, Y. Tsunobuchi, et al., Nat. Chem. **3**, 564 (2011).
4. S. V. Streltsov and D. I. Khomskii, Phys. Usp. **60**, 1121 (2017).
5. T. Saha-Dasgupta and P. Oppeneer, MRS Bull. **39**, 614 (2014).
6. C. M. Jureschi, J. Linares, A. Rotaru, et al., Sensors **15**, 2388 (2015).
7. R. M. Wentzcovitch, J. F. Justo, Z. Wu, et al., Proc. Natl. Acad. Sci. U. S. A. **106**, 8447 (2009).
8. S. G. Ovchinnikov, T. M. Ovchinnikova, P. G. Dyad'kov, V. V. Plotkin, and K. D. Litasov, JETP Lett. **96**, 129 (2012).
9. R. Sinmyo, C. Mccammon, and L. Dubrovinsky, Am. Mineralog. 102, 1263 (2017).
10. S. V. Streltsov, A. O. Shorikov, S. L. Skornyakov, et al., Sci. Rep. **7**, 13005 (2017).
11. A. I. Nesterov, Yu. S. Orlov, S. G. Ovchinnikov, and S. V. Nikolaev, Phys. Rev. B **96**, 134103 (2017).
12. I. S. Lyubutin, V. V. Struzhkin, A. A. Mironovich, et al., Proc. Natl. Acad. Sci. U. S. A. **110**, 7142 (2013).
13. M. M. Korshunov, V. A. Gavrichkov, S. G. Ovchinnikov, Z. V. Pchelkina, I. A. Nekrasov, M. A. Korotin, and V. I. Anisimov, J. Exp. Theor. Phys. **99**, 559 (2004).
14. V. V. Val'kov and S. G. Ovchinnikov, Sov. J. Theor. Math. Phys. **50**, 306 (1982).
15. V. A. Gavrichkov, S. I. Polukeev, and S. G. Ovchinnikov, J. Exp. Theor. Phys. **127**, 713 (2018).
16. N. O. Lipari, C. B. Duke, and L. Pietronero, J. Chem. Phys. **65**, 1165 (1976).
17. A. Painelli and A. Girlando, J. Chem. Phys. **84**, 5655 (1986).
18. Yu. S. Orlov, L. A. Solovyev, V. A. Dudnikov, et al., Phys. Rev. B **88**, 235105 (2013).
19. A. I. Nesterov and S. G. Ovchinnikov, JETP Lett. **90**, 530 (2009).
20. A. G. Gavriliuk, I. A. Trojan, I. S. Lyubutin, S. G. Ovchinnikov, and V. A. Sarkissian, J. Exp. Theor. Phys. **100**, 688 (2005).
21. D. M. Wilson and S. Broersma, Phys. Rev. B **14**, 1977 (1976).
22. M. J. Massey, R. Merlin, and S. M. Girvin, Phys. Rev. Lett. **69**, 2299 (1992).
23. V. A. Sarkisyan, I. A. Troyan, I. S. Lyubutin, A. G. Gavrilyuk, and A. F. Kashuba, JETP Lett. **76**, 664 (2002).
24. A. G. Gavriliuk, I. A. Trojan, R. Boehler, M. Eremets, A. Zerr, I. S. Lyubutin, and V. A. Sarkisyan, JETP Lett. **75**, 23 (2002).
25. I. A. Troyan, M. I. Eremets, A. G. Gavrilyuk, I. S. Lyubutin, and V. A. Sarkisyan, JETP Lett. **78**, 13 (2003).
26. S. G. Ovchinnikov, JETP Lett. **77**, 676 (2003).
27. S. G. Ovchinnikov and V. N. Zabluda, J. Exp. Theor. Phys. **98**, 135 (2004).
28. K. Parlinski, Eur. Phys. J. B **27**, 283 (2002).
29. A. G. Gavriliuk, I. A. Trojan, S. G. Ovchinnikov, I. S. Lyubutin, and V. A. Sarkisyan, J. Exp. Theor. Phys. **99**, 566 (2004).
30. I. A. Troyan, A. G. Gavrilyuk, S. G. Ovchinnikov, I. S. Lyubutin, and N. V. Kazak, JETP Lett. **94**, 748 (2011).
31. A. P. Drozdov, M. I. Eremets, I. A. Troyan, V. Ksenofontov, and S. I. Shylin, Nature (London, U.K.) **525**, 73 (2015).
32. I. Troyan, A. Gavriliuk, R. Ruffer, A. Chumakov, A. Mironovich, I. Lyubutin, D. Perekalin, A. Drozdov, and M. Eremets, Science (Washington, DC, U. S.) **351** (6279), 1303 (2016).
33. M. Somayazulu, M. Ahart, A. K. Mishra, Z. M. Geballe, M. Baldini, Y. Meng, V. V. Struzhkin, and R. J. Hemley, Phys. Rev. Lett. **122**, 027001 (2019).

Translated by N. Wadhwa